LRP 609/98 June 1998

SUITABILITY OF DRIFT NONLINEARITY IN SI, GAAS AND INP FOR HIGH POWER FREQUENCY CONVERTERS WITH A 1 THZ RADIATION OUTPUT

R. Brazis, R. Raguotis, M.R. Siegrist

Accepted for publication in
J. Appl. Phys.

Suitability of drift nonlinearity in Si, GaAs and InP for high power frequency converters with a 1 THz radiation output

R. Brazis, R. Raguotis

Semiconductor Physics Institute (SPI),

A. Gostauto 11, LT-2600 Vilnius, Lithuania

M. R. Siegrist

Centre de Recherches en Physique des Plasmas (CRPP),

Association Euratom - Confédération Suisse,

Ecole Polytechnique Fédérale de Lausanne,

PPB Ecublens, 1015 Lausanne, Switzerland

Abstract

We investigate the nonlinear drift response of electrons in Si, GaAs and InP crystals to high-power electromagnetic waves by means of a Monte Carlo technique, with the aim of developing an efficient frequency converter for 1 THz output radiation. Drift velocity amplitudes and phases determining the conversion efficiency are calculated for the 1st, 3rd- and 5th harmonics in the pumping wave amplitude range of $10 < E_1 < 100$ kV/cm, for frequencies between 30 and 500 GHz, and at the lattice temperatures of 80, 300 and 400 K. It is found that the efficiency is a maximum at the pumping wave amplitude of the order of 10 kV/cm depending on the intervalley electron scattering parameters and the lattice temperature. Cooling the nonlinear crystal down to the liquid nitrogen temperature enhances the efficiency several times in Si and by orders of magnitude in GaAs and InP. This is promising for obtaining a 10 percent conversion efficiency.

1. Introduction

Powerful cw or quasi-cw power sources in the 1 THz frequency domain are required for plasma diagnostic purposes, in particular for collective Thomson scattering of a α-particles[1] or some other applications such as high frequency radar. Apart from the free electron lasers no such sources are currently available. Existing gyrotrons are able to deliver powers in the MW range, but not at these high frequencies, which either requires very high magnetic fields or operation at higher harmonics with correspondingly reduced efficiency. However, existing gyrotrons around 200 to 300 GHz, followed by a passive frequency multiplier, which converts the radiation into the third or fifth harmonic, might be a suitable solution. Such a scheme would only be of interest if the efficiency of the converter reached at least 10% and were able to handle the power absorbed at the fundamental frequency.

Previous theoretical and experimental investigations[2-9] have shown that different semiconductor materials exhibit significant gain at higher harmonics in the frequency range of interest. However, the highest efficiency achieved so far was only 0.1% in the normal incidence experiments on n-type silicon plates[6-9]. The limitations were given by a surface breakdown effect which precluded pumping of the material with higher powers, and by saturation effects observed below the breakdown threshold. Considerably higher nonlinear susceptibilities need to be revealed if the problem is to be solved by judicious choice of material alone.

The present paper remaining in the framework of the drift nonlinearity aims to explore the efficiency of technologically important materials on the basis of Monte Carlo simulations.

The paper presents the details of the problem formulation (Sec. 2), the results of Monte Carlo simulations (Sec. 3), and the discussion of possible experimental realizations (Sec. 4).

2. Problem formulation

The primary idea[2] of efficient harmonic generation is based on the cubic relation between the forward-emitted 3rd harmonic intensity I_3 and the pumping wave intensity I_1 incident on a slab of thickness d

$$I_3 = \frac{32\pi}{c}\left|T_c \chi_3 C(d)\right|^2 I_1^3, \tag{1}$$

where c is the speed of light, χ_3 is the third-order nonlinear susceptibility understood as the coefficient in the expansion of the polarization $\boldsymbol{P} = \chi_1 \boldsymbol{E} + (\chi_3 E^2)\boldsymbol{E} + \ldots$ in the power series of electric field $\boldsymbol{E}$, T_c is the factor of the electric field amplitude change when crossing the front and back boundaries of the slab[9],

$$T_c = \frac{2\sqrt{\varepsilon_3}}{1+\sqrt{\varepsilon_3}}\left(\frac{2}{1+\sqrt{\varepsilon_1}}\right)^3, \tag{2}$$

and $C(d)$ is the thickness-dependent phase matching factor[9]

$$C(d) = \frac{e^{i3k_1 d} - e^{ik_3 d}}{\varepsilon_1 - \varepsilon_3}, \tag{3}$$

where ε_N is the dielectric permeability at the Nth harmonic frequency, and $\boldsymbol{k}_N$ is the Nth harmonic wave vector.

If the 3rd order susceptibility as well as T_c and $C(d)$ are independent of the wave amplitude, then Eq.(1) implies that a sufficiently high pump intensity is all that is required to obtain high intensity and efficiency of 3rd harmonic generation. In contrast to this, experiments on n-type Si

crystals have shown that the 3rd harmonic intensity deviates from the cubic increase and finally saturates with rising pump wave intensity. The cause of saturation is found in the change of electron scattering and their effective mass in the high-amplitude pumping wave electric field.

The problem is to find semiconductor materials and/or operating temperatures which result in higher third harmonic generation (THG) efficiency. Let us consider electrons in the conduction band as the only source of non-linearity. Assuming constant electron density, we focus our attention on the drift non-linearity. Monte Carlo modeling provides the time dependence of the drift velocity $V(t)$ of electrons in the pumping wave field varying in time as $E_1\cos\omega_1 t$. Fourier-transformation applied to $V(t)$ then gives the drift velocity components $V_N\cos(\omega_N t + \psi_N)$ where ψ_N is the drift velocity phase. Following the relation $\partial P/\partial t = neV$, where e is the elementary charge, one gets the equivalence[8]

$$\chi_3 = i\frac{ne}{3\omega_1\varepsilon_0 E_1^2}\left(\frac{V_3}{E_1}\right), \tag{4}$$

where ε_0 is the free-space dielectric constant, and the ratio of V_3 and E_1 is complex due to the phase shift. The 3rd harmonic intensity is now

$$I_3 = K_0\left|\frac{ne}{\omega_1}\frac{2}{1+\sqrt{\varepsilon_1}}\frac{2\sqrt{\varepsilon_3}}{1+\sqrt{\varepsilon_3}}\frac{V_3}{E_1}C(d)\right|^2 I_1, \tag{5}$$

where K_0 is the material- and field-independent constant, ε_1 is the complex permeability at the pumping wave frequency,

$$\varepsilon_1 = \varepsilon_L + i\frac{ne}{\omega_1\varepsilon_0 E_1^2}\left(\frac{V_1}{E_1}\right), \tag{6}$$

where ε_L is the lattice dielectric permeability, and the ratio of V_1 and E_1 is complex due to the phase shift. The complex permeability at the 3rd harmonic frequency is approximated as

$$\varepsilon_3 \approx \varepsilon_L + i\frac{ne}{3\omega_1\varepsilon_0}\mathrm{Re}\left(\frac{V_1}{E_1}\right)\left[1 - i\frac{3\omega_1 m^*}{e}\mathrm{Re}\left(\frac{V_1}{E_1}\right)\right]^{-1}, \tag{7}$$

where $Re(V_1/E_1)$ is the real part of the complex ratio, and m^* is the electron effective mass.

The function $C(d)$ in low-loss materials exhibits Maker's oscillations[10] when the sample thickness is subject to monotonous change. In highly absorbing materials the function shows a single maximum at a certain sample thickness mainly determined by the loss: therefore the maximum does not present any guide for the harmonic output optimization in this case. Instead of seeking for a thickness-controlled maximum, we focus here on thin samples so as to reduce the Joule loss, and to reveal electronic factors controlling the output power and efficiency. With the assumptions that the free-electron contribution in Eqs (6) and (7) is small compared to the lattice one, and the slab thickness d is small enough to satisfy the condition

$$d \ll \sqrt{\frac{\varepsilon_L}{\mu_0}\frac{2}{ne}\left(\frac{E_1}{V_1}\right)}, \tag{8}$$

where μ_0 is the free-space magnetic constant, the 3rd harmonic intensity can be expressed as

$$I_3 = K_0'\left(\frac{2}{1+\sqrt{\varepsilon_L}}\right)^2\left|\frac{endV_3}{E_1}\right|^2 I_1, \tag{9}$$

where K_0' is the modified physical constant independent of the material and field parameters. The last expression states that the efficiency $\eta_3 = I_3/I_1$ is proportional to the square of the 3rd harmonic surface current density at a given pumping wave amplitude. If the surface carrier density nd is constant, the 3rd harmonic output power is governed by the 3rd harmonic drift

velocity amplitude at the pumping wave field amplitude E_1. The same is true for the 5th harmonic conversion efficiency.

We determine the 3rd and 5th harmonic drift velocity dependencies on E_1 using Monte Carlo techniques. The algorithm of MC simulations in an alternating electric field follows the standard procedure[11]. It involves the intra- and intervalley scattering of electrons, and the band nonparabolicity. We do not re-write here the basic equations for the scattering rates which are presented elsewhere[12]. The upper limit for the pumping field amplitude is taken to be 100 kV/cm. At higher fields a time-consuming full-band modeling would be required[13] to account for electron access to higher energy bands in the momentum space. However, the harmonic intensity saturation and the efficiency decrease with the rise of the pumping wave field amplitude starts at much lower amplitudes, making the upper limit of $E_1 \leq 100$ kV/cm reasonable. At low pump field amplitudes ($E_1 < 10$ kV/cm) the Monte Carlo procedure is exceedingly slow and hence this region was not investigated.

3. Results and discussion

3.1. Silicon

The indirect energy gap of bulk silicon crystals is 1.124 eV at T = 300 K[14] allowing to apply electric fields up to 100 kV/cm before the onset of impact avalanche processes. The lowest conduction band minima are located at the X-points of the Brillouin zone, the constant energy surfaces in the vicinity of these points are ellipsoidal, and the energy dependence on momentum is non-parabolic.

The bulk crystals of n-type silicon are represented by six ellipsoidal X-valleys for electrons taking into account the nonparabolicity. At room temperature, the electron intravalley scattering

is modeled including one type of acoustic phonons in the equipartition and elastic approximation employing a deformation potential. The intervalley scattering is accounted for by six types of large-momentum zone-boundary phonons[15] (Table I). Earlier results of Monte Carlo modeling for n-type Si have been directly compared with experimental data on the 3rd harmonic generation at room temperature showing very good agreement[8,9]. The maximum experimental efficiency was about 0.1 percent. We investigate now the amplitude- and frequency dependencies of the drift response at the lattice temperatures T = 80 and 400 K, and compare them with the data for T = 300 K. The lower temperature is representative of a situation where the crystal is cooled down to liquid nitrogen temperature, whereas 400 K is a typical value in a room temperature experiment, assuming the crystal has been heated up by a cw or long pulse pump beam. We compare also the 3rd harmonic with the 5th harmonic. The latter would allow us to use lower pumping wave frequencies.

The result of cooling down the crystal to liquid nitrogen temperature is a 1.5 to 2 times higher third harmonic drift velocity amplitude (Fig.1). Rising the lattice temperature to 400 K, on the other hand, results in a decrease of the harmonic amplitude. The 3rd harmonic phase is most sensitive to the pumping wave field amplitude when the lattice temperature is T = 80 K (Fig. 2) whereas the 1st harmonic phase is much less sensitive both to the pumping wave field amplitude and to the lattice temperature.

The 5th harmonic drift velocity amplitude at T = 80 K (Fig. 3) is nearly equal to the 3rd harmonic amplitude at T = 400 K (cf. Fig.1). This means that an appreciable 1 THz output wave can be obtained in silicon crystals by using a lower-frequency pumping source. The 5th harmonic phase is much more sensitive to the pumping wave field amplitude than that of the 3rd harmonic (Fig. 4) imposing more strict requirements on the spatial uniformity of the pump wave amplitude for optimum output. On the other hand, it is a remarkable feature for device applications implying phase modulation of the harmonic radiation.

The 3rd harmonic drift velocity amplitude decreases with pumping wave frequency both at T = 80 K and at 300 K (Figs 5 and 6). At T = 400 K the same tendency is observed at low pumping wave amplitudes only. It is seen that both an increase of lattice temperature and pumping wave field amplitude results in reduced dispersion of the 3rd harmonic drift velocity. The effects of increasing lattice temperature are seen to be similar to those of increasing electron temperature which grows with pumping wave amplitude[8]. The 5th harmonic drift velocity exhibits much more pronounced dispersion than the 3rd harmonic one (Figs 5,6) whereas the 1st harmonic is nearly dispersionless.

Note that the electric field vector in the present Monte Carlo simulations was assumed to be parallel to the [100] direction, as it was in previous experiments[5-9].The fundamental frequency in those experiments was 442 GHz, i.e., somewhat higher than that considered in the present work. The Monte Carlo data show that the frequency decrease from 442 GHz to 333 GHz does not significantly affect the 3rd harmonic generation efficiency in n-type Si. Experiments at the pump wave frequency of 600 GHz have shown[3] that the 3rd order susceptibility of n-type Si at T = 300 K is $\chi_3 = 10^{-16} \mathrm{m}^2/\mathrm{V}^2$ for $n = 10^{14}$ cm^{-3}, and it varies linearly with the rise of the carrier density. This is in fairly good agreement with the extrapolated data on the third harmonic drift velocity (Fig.1) at E_1 = 100 kV/cm inserted into Eq. (4).

In Fig. 7 we present the third harmonic conversion efficiency, normalized to the maximum at 300 K, as function of the pump wave amplitude. Maximum efficiency is obtained at about 10% of the highest pump power level investigated. The efficiency decreases nearly 3 times when the power approaches this maximum value. Cooling the crystal down to T = 80 K results in 4 times higher efficiency at the maximum (or nearly 10 times compared to the efficiency at the highest power level at room temperature). Thus cooling the crystal down to liquid nitrogen temperature together with the use of reduced pumping power results in a 3rd harmonic efficiency enhanced

by an order of magnitude compared to that observed at high pump power levels. It still does not meet the requirement of 10% efficiency and other materials need to be investigated.

3.2. Gallium arsenide

The energy gap in GaAs crystals (1.429 eV at T = 300 K)[14] is higher than that in Si allowing for higher electric field application below the impact avalanche threshold. Thermal equilibrium electrons in the conduction band of GaAs crystals are located at the central Γ-valley. They are expected to exhibit an enhanced non-linearity in high electric fields due to the transfer between the numerous (Γ-, L-, and X-) valleys. Monte Carlo simulations of the drift response to the microwave electric field have been reported earlier[16] at low electric field amplitudes (E_1 < 20 kV/cm) and frequencies (ν_1< 135 GHz). One can deduce from those data that the 3rd harmonic amplitude increases and the 1st harmonic one decreases with rising pumping wave field amplitude presenting a favorable feature for the harmonic generation. However, the coupling constants used in the modeling turned out to be different from that deduced from the existing experimental works. Experiments on n-type GaAs in the millimeter wave range[17,18] have shown third harmonic emission; however, they have been focused rather on resonant phenomena than on a high power output. Therefore, it was necessary to renew the Monte Carlo simulation, expanding its limits to higher frequencies and field amplitudes.

The set of n-type GaAs parameters used in the present work is given in Table II. We focus on the region of high amplitudes of the pumping wave field, omitting the "ohmic" part of the V_1-E_1 characteristics. In contrast to Si crystals, gallium arsenide exhibits a negative slope of the V_1-E_1 characteristics (Fig. 8). It indicates that the electron transfer from the Γ-valley to higher (X- and L-valleys) is effective even at these quite high frequencies of the pumping wave. The negative slope has been observed in dc measurements[20] and microwave experiments at low

frequencies[21]. There are no experimental data on the high-field response at the frequencies we are interested in.

The 3rd harmonic drift velocity amplitude at $T = 80$ K shows an especially interesting feature: it is nearly independent of the pumping field amplitude above 20 kV/cm and is much higher than that in n-type Si. At $T = 300$ K, the 3rd harmonic drift velocity amplitude in GaAs is higher than that in Si only in the region of low pumping field amplitudes. Harmonic phase behavior in n-type GaAs is similar to that in n-type Si.

The 5th harmonic drift velocity amplitude in GaAs at $T = 80$ K (Fig. 9) is significantly higher than in Si. It is equal to the 3rd harmonic amplitude in Si at $T = 300$ K in the region of high pumping wave amplitudes. Moreover, the 5th harmonic in GaAs at $T = 80$ K is higher than the 3rd harmonic in Si at $T = 300$ K in the range of lower pumping field amplitudes. This means that the 1 THz radiation in GaAs can be obtained employing lower-frequency pumping wave sources. However, the 5th harmonic phase in GaAs is quite sensitive to the pumping wave amplitude in accordance with what is observed in Si.

The drift velocity amplitude dispersion in GaAs (Figs 10,11) shows some peculiarities not encountered in Si, e.g. the slightly positive dispersion of the 1st harmonic drift velocity at low field amplitudes ($E_1 = 10$ kV/cm, dashed lines in Figs 10,11). It can be attributed to the inertia of electrons which becomes more pronounced with the rise of frequency. Another effect is the higher harmonic amplitude cross-over which takes place, e.g., at $n_1 \approx 160$ GHz for the 3rd harmonic at $T = 80$ K. At this pumping wave frequency the harmonic drift velocity amplitude does not depend on the pumping wave amplitude in the range of $10 < E_1 < 100$ kV/cm. At pumping wave frequencies below the cross-over point the drift velocity harmonic amplitudes *decrease* with the rise of the pump wave electric field amplitude, whereas at frequencies above the cross-over point the drift velocity harmonic amplitudes *grow* with the rise of pumping field.

The 3rd harmonic cross-over point shifts to lower frequencies and broadens slightly to cover a range of frequencies with the rise of temperature (Figs 10,11). The cross-over point for the 5th harmonic at $T = 80$ K is at $\nu_1 \approx 60$ GHz. It shifts and broadens with rising temperature as well.

The relative efficiency of the 3rd harmonic generation in GaAs at $T = 80$ and 300 K is shown in Fig. 7. One can judge that, similarly to the case of silicon, an exceedingly high pump power results in diminishing efficiency. The maximum efficiency is at the pump wave amplitude of $E_1 \approx 10$ to 15 kV/cm, depending on the lattice temperature.

3.3. Indium phosphide

The band structure of InP crystals is similar to that of GaAs but the energy gap is slightly smaller (1.344 eV at $T = 300$ K)[14]. The energy separation between the lowest and upper valleys in the conduction band, as well as the relevant phonon energies are somewhat higher (Table III). Therefore one can expect an enhanced harmonic generation related to the intervalley electron transfer. We examine this assumption using the same Monte Carlo procedure.

The 3rd harmonic drift velocity amplitude in n-type InP at $T = 80$ K (Fig. 12) is only slightly higher than in GaAs (Fig. 7) and nearly 1.5 times higher than in Si (Fig.1). The advantage of InP is seen in significantly higher harmonic amplitudes at $T = 300$ and 400 K, as compared to those in GaAs or Si. The 3rd harmonic phase behavior at $E_1 < 20$ kV/cm (Fig.13) is more complicated than in GaAs or Si. The 5th harmonic drift velocity amplitude in InP at $T = 80$ K (Fig.14) is higher than the 3rd harmonic in Si at $T = 300$ K. Even at temperatures of 300 to 400 K the 5th harmonic in InP is nearly the same as the 3rd one in Si at room temperature. This is a promising peculiarity for frequency up-converters operating at comparatively low pumping frequency. A complicated behavior of the 5th harmonic amplitude and phase is seen in the range of the pumping field amplitudes below 30 kV/cm (Figs 14 and 15). Most likely, it is related to

electron runaway from the Γ-valley to upper valleys which starts at higher field amplitudes as compared to GaAs because of the higher separation between the valleys. The 1st harmonic drift velocity amplitude dispersion in InP crystals is negligible (Figs 16,17). The 3rd harmonic amplitude decreases 2 to 3 times, and the 5th harmonic amplitude decreases up to 10 times with a pumping frequency rise from 30 to 500 GHz. The cross-over points of the dispersion curves calculated for $E_1 = 40$ and 100 kV/cm are shifted to much higher frequencies, compared to that in GaAs (Figs 16,17 and 10,11). At low pumping field amplitudes the dispersion characteristics of higher harmonics in InP do not cross those belonging to high pumping field amplitudes. This means that electrons in InP remain in the central valley up to much higher field amplitudes as compared to GaAs.

The 3rd harmonic generation efficiency in InP is compared to that in Si and GaAs crystals in Fig. 7. It is seen that InP at $T = 300$ K is nearly as good a nonlinear crystal as GaAs at $T = 80$ K. Gallium arsenide is superior in the range of the pumping field amplitudes up to 30 kV/cm, whereas InP is somewhat better in the range of $E_1 = 40$ to 50 kV/cm. Indium phosphide seems to beat other candidate materials for frequency tripling at $T = 80$ K (Fig. 7) for $E_1 > 20$ kV/cm.

3.4 Joule loss

The problem of heat removal is crucial for the cw operation of frequency converters. Sample heating by the pumping wave reduces the efficiency, as is seen from the temperature dependence of efficiency. It can cause thermal activation of electrons and holes resulting in heavy loss and severely reduced penetration of the pumping wave in the non-linear crystal. It is interesting to compare the heat production per electron in Si, GaAs, and InP. This has been calculated as $V_1 E_1 \cos\psi_1$. The results show that the loss in InP at $T = 80$ K in the field amplitude range where the 3rd harmonic generation efficiency is a maximum does not exceed that in GaAs

(Fig. 18). The loss at the maximum efficiency is 2.5 times higher than that in n-type Si at T = 300 K.

It has to be emphasized that the linear absorption per electron in all the crystals is quite high and hence an efficient harmonic generation can only be considered in thin layers, in agreement with the assumption this paper is based on. The active layer needs to be deposited on a highly transparent thermal conductor. This is feasible in epitaxial active layers on insulating substrates of the same material.

The thermal conductivity of Si is 14.5 W/(cm K) at T = 80 K and 1.56 W/(cm K) at 300 K[14]. At liquid nitrogen temperature it is even higher than that of copper[22], presenting a favorable feature for heat extraction: it facilitates an intense thermal flow to the bath. On the other hand, GaAs and InP crystals are more efficient than Si and less sensitive to thermal generation of carriers or electric breakdown owing to their larger energy gap between the valence and conduction bands. The thermal conductivity of GaAs (4.3 W/(cm K) at T = 80 K and 0.58 W/(cm K) at 300 K)[14] is 3 times lower than that of Si, whereas InP crystals present somewhat better values of 5.2 W/(cm K) at T = 80 K and 0.7 W/(cm K) at 300 K[14]. Thus, some complications incurred by cooling down the crystals to 80 K can be justified, especially when one takes into account the resulting improvement both of the harmonic generation efficiency and the Joule heat transfer.

4. Conclusion

On the basis of Monte Carlo modeling we find that silicon, a readily available and simple to use material, is nearly as good as n-type GaAs or InP, as far as efficiency at high power is concerned. However, much higher efficiency in GaAs and InP as compared to Si is expected at relatively low pumping power levels. The 3rd harmonic generation efficiency can probably be

raised up to 10 percent employing pure n-type GaAs or n-type InP crystals cooled down to liquid nitrogen temperatures. The 5th order nonlinearity of InP turns out to be competitive too.

Phase synchronism is important for frequency up-conversion. In the case of the harmonic generation along the pumping wave path in a crystal, the harmonic- and the pumping wave phases are subject to spatial change related to the amplitude variation. This, together with the Joule heat production, limits the useful thickness of a non-linear crystal plate. The output power optimization can therefore not be achieved by using thick samples. Instead of this, thin non-linear layers in a resonant cavity seem to be advantageous. Insertion of the converter into a resonant structure should enable us to extract a much larger fraction of the stored energy by passing the harmonic radiation repetitively through the same active layer. Hereby the thickness of the active material should be chosen small enough to reduce the Joule loss and achieve an optimal gain during each pass; a parameter which is mainly determined by the phase relationship between fundamental and harmonic waves[23]. Since a free-standing thin layer in a cavity is difficult to cool, epitaxial layers on insulating substrates have to be considered.

The cavity must provide the possibility of independent phase control for the pumping- and the harmonic waves. This is difficult to realize in pulsed operation because the phases are subject to dramatic change with the field amplitudes. The same is true for the transient build-up during cw operation. The cavity needs to be readjusted with the change of cw operation power level.

The problem of heat removal is crucial for the cw operation of the frequency converters. Sample heating by the pumping wave reduces the efficiency. It can cause thermal activation of electrons and holes resulting in heavy loss and severely reduced penetration of the pumping wave into the non-linear crystal. This is especially critical in narrow-gap materials. By cooling down to liquid nitrogen temperatures the harmonic generation efficiency is improved by orders of magnitude. The thermal conductivity of semiconductor crystals at low temperatures results in

an intense thermal flow to the bath. GaAs and InP crystals are more efficient than Si and less sensitive to overheating or electric breakdown owing to their larger energy gap between the valence and conduction bands.

Concerning further Monte Carlo modeling, wide-gap materials with even higher energy distance between the fundamental and upper valleys like silicon carbide or gallium nitride seem to be prospective candidates for high-temperature operation of high-power harmonic radiation sources.

Acknowledgment

This work was partly supported by the Swiss National Science Foundation.

References

1. R. Behn, D. Dicken, J. Hackmann, S. A. Salito, M. R. Siegrist, P. A. Krug, I. Kjelberg, B. Duval, B. Joye and A. Pochelon, Phys. Rev. Lett. **62,** 2833 (1989).
2. F. Keilmann, Proc. SPIE, **666**, 193 (1986).
3. A. Mayer and F. Keilmann, Phys. Rev. B, **33,** 6962 (1989).
4. F. Keilmann, R. Brazis, H. Barkley, W. Kasparek, M. Thumm and V. Erckmann, Europhys. Letters, **11**(4), 337 (1990).
5. M. R. Siegrist, F. Keilmann, Ch. Nieswand and M. Urban, Infrared Physics and Technology, **36**, 407 (1995).
6. M. Urban, Ch. Nieswand, M. R. Siegrist and F. Keilmann, J. Appl. Phys. **77**, 981 (1995).
7. M. Urban, M. R. Siegrist, L. Asadauskas, R. Raguotis and R. Brazis, Lithuanian Journal of Physics, **35**, 430 (1995).
8. M. Urban, M. R. Siegrist, L. Asadauskas, R. Raguotis and R. Brazis, Appl. Phys. Lett., **69**, 1776 (1996).
9. M. Urban, *Third harmonic generation of high power far infrared radiation in semiconductors*, Dr sci. thesis No 1492, EPFL, Lausanne, 1996, 105 p.
10. R. W. Terhune, P. D. Maker and C. M. Savage, Phys. Rev. Lett., **8**, 404 (1962).
11. P. A. Lebwohl, J. Appl. Phys. **44**, 1744 (1979).
12. C. Jacoboni and P. Lugli, *The Monte Carlo Method for Semiconductor Device Simulation*, Springer Verlag, Wien, 1989.
13. T. Kunikiyo, M. Takenaka, Y. Kamakura, M. Yamaji, H. Mizuno, M. Morifuji, K. Taniguchi and C. Hamaguchi, J. Appl. Phys. **75** (1), 297 (1994).
14. A. Dargys and J. Kundrotas, *Handbook on physical properties of Ge, Si, GaAs and InP*, Sci. and Encyclopedia Publishers, Vilnius, 1994, 266 p.

15. R. Brunetti, C. Jacoboni, T. Nava, L. Reggiani, G. Bosman and R. J. J. Zijlstra , J. Appl. Phys., **52**, 6713 (1981).

16. R. Raguotis and A. Reklaitis, Phys. Stat. Sol. (a), **62**, 399 (1980).

17. R. Brazis and A. Mironas, Fizika i Tekhnika Poluprovodnikov, **17**(4), 720 (1983); *Engl. transl.*: Soviet Phys.- Semiconductors, **17**(4), 450 (1983).

18. V. Ambrazeviciene, R. Brazis and A. Kunigelis, in: *Nonlinear surface electromagnetic phenomena, Chapt. 6*, eds.: Ponath and G. Stegeman, Elsevier, North Holland, 1991.

19. K. Brennan and K. Hess, Solid-State Electronics, **27,** 347 (1984).

20. C. S. Chang and H. R. Fetterman, Solid State Electronics, **29**, 1295 (1986).

21. G. Hill and P. N. Robson, Solid State Electronics, **25**, 589 (1982).

22. S. M. Sze, *Physics of semiconductor devices*, Wiley &Sons, 1981.

23. R. Brazis, R. Raguotis, L. Asadauskas and M. R. Siegrist, Int. J. IR and MM Waves, **18**(6), 1217 (1997).

Table I. Selected parameters of silicon crystals[a]

Density: 2.33 g/cm^3

Longitudinal sound velocity: 9 km/s

Lattice dielectric permeability (static):11.3

	X valley
Number of valleys	6
Location in k-space	$k = 0.85k_{max}$ [100]
Nonparabolicity coef., eV^{-1}	0.5
Uniax. deformation potential, eV	9
Electron effective mass:	
longitudinal, m_0	0.9
transverse, m_0	0.192

Phonon parameters for electron scattering in silicon[b]:

Phonon type	Phonon energy, meV	Electron-phonon coupling constant, 10^8 eV/cm
f	19	0.3
f	47.4	2.0
f	59	2.0
g	12	0.5
g	18.5	0.8
g	62	11

[a]Ref. 14 [b]Ref. 15

Table II. Selected GaAs crystal parameters[a]

Density: 5.32 g/cm^3

Longitudinal sound velocity: 5.24 km/s

Lattice dielectric permeability (static):12.8 ; (optic):10.9

	X valley	L valley	Γ valley
Number of valleys	3	4	1
Valley location in ***k***-space	k=0.9k_{max}	$k = k_{max}$	$k = 0$
	[100]	[111]	
Energy separation, eV	0.52	0.33	0
Nonparabolicity coef., eV^{-1}	0.36	0.65	0.69
Uniax. deformation potential, eV	8	8	8
Optical phonon energy, meV	35	35	35
Electron effective mass, m_0	0.43	0.23	0.063

Intervalley scattering parameters[b]

Transition	Phonon energy, meV	Electron-phonon coupling constant, 10^8 eV/cm
Γ-L	26	10
Γ-X	26	10
L-L	26	10
L-X	26	9
X-X	26	9

[a]Ref. 14 [b]Ref. 19

Table III. Selected InP crystal parameters[a]

Density: 4.8 g/cm^3

Longitudinal sound velocity: 5.13 km/s

Lattice dielectric permeability (static):12.35; (optic): 9.52

	X valley	L valley	Γ valley
Number of valleys	3	4	1
Valley location in ***k***-space	$k = 0.9k_{max}$ [100]	$k = k_{max}$ [111]	$k = 0$
Energy separation, eV	0.775	0.54	0
Nonparabolicity coef., eV^{-1}	0.38	0.23	0.83
Uniax. deformation potential, eV	6.5	14.5	8
Optical phonon energy, meV	43	43	43
Electron effective mass, m_0	0.325	0.26	0.078

Intervalley scattering parameters[b]:

Transition	Phonon energy, meV	Electron-phonon coupling constant, 10^8 eV/cm
Γ-L	27.8	10
Γ-X	29.9	10
L-L	29	10
L-X	29.3	9
X-X	29.9	9

[a]Ref. 14 [b]Ref. 19

Figure captions

Fig. 1. Drift velocity amplitude of the first (1) and the third (3) harmonics of 333 GHz in n-type Si as a function of the electric field amplitude. The curve labels give the lattice temperatures (in K).

Fig. 2. Drift velocity phase of the first (1) and the third (3) harmonics of 333 GHz in n-type Si as a function of the electric field amplitude. The curve labels give the lattice temperatures (in K).

Fig. 3. Drift velocity amplitude of the first (1) and the fifth (5) harmonics of 200 GHz in n-type Si as a function of the electric field amplitude. The curve labels give the lattice temperatures (in K).

Fig. 4. Drift velocity phase of the first (1) and the fifth (5) harmonics of 200 GHz in n-type Si as a function of the electric field amplitude. The curve labels give the lattice temperatures (in K).

Fig. 5. The 3rd harmonic drift velocity amplitude (solid line) as a function of the pump wave frequency in n-type Si at the lattice temperature of 80 K. The curve labels give the wave electric field amplitudes (in kV/cm). The 1st- (dashed line) and the 5th (dotted line) harmonic drift velocity amplitudes are shown for comparison.

Fig. 6. The 3rd harmonic drift velocity amplitude (solid line) as a function of the pump wave frequency in n-type Si at the lattice temperature of 300 K. The curve labels give the wave electric field amplitudes (in kV/cm). The 1st (dashed line) and the 5th (dotted line) harmonic drift velocity amplitudes are shown for comparison.

Fig. 7. THG efficiency divided by the maximum efficiency of n-type Si at $T = 300$ K as a function of the pumping wave amplitude. The curve labels give materials and lattice temperatures. The pump wave frequency is 333 GHz.

Fig. 8. Drift velocity amplitude of the first (1) and the third (3) harmonics of 333 GHz in n-type GaAs as a function of the electric field amplitude. The curve labels give the lattice temperatures (in K).

Fig. 9. Drift velocity amplitude of the first (1) and the fifth (5) harmonics of 200 GHz in n-type GaAs as a function of the electric field amplitude. The curve labels give the lattice temperatures (in K).

Fig. 10. The 3rd harmonic drift velocity amplitude (solid line) as a function of the pumping wave frequency in n-type GaAs at $T = 80$ K. The curve labels give the wave electric field amplitudes (in kV/cm). The 1st (dashed line) and the 5th (dotted line) drift velocity harmonic amplitudes are shown for comparison.

Fig. 11. The 3rd harmonic drift velocity amplitude (solid line) as a function of the pumping wave frequency in n-type GaAs at $T = 300$ K. The curve labels give the wave electric field amplitudes (in kV/cm). The 1st (dashed line) and the 5th (dotted line) drift velocity harmonic amplitudes are shown for comparison.

Fig.12. Drift velocity amplitude of the first (1) and the third (3) harmonics of 333 GHz in n-type InP as a function of the electric field amplitude. The curve labels give the lattice temperatures (in K).

Fig.13. Drift velocity phase of the first (1) and the third (3) harmonics of 333 GHz in n-type InP as a function of the electric field amplitude. The curve labels give the lattice temperatures (in K).

Fig.14. Drift velocity amplitude of the first (1) and the fifth (5) harmonics of 200 GHz in n-type InP as a function of the electric field amplitude. The curve labels give the lattice temperatures (in K).

Fig. 15. Drift velocity phase of the first (1) and the fifth (5) harmonics of 200 GHz in n-type InP as a function of the electric field amplitude. The curve labels give the lattice temperatures (in K).

Fig. 16. The 3rd harmonic drift velocity amplitude (solid line) as a function of the pumping wave frequency in n-type InP at $T = 80$ K. The curve labels give the wave electric field amplitude (in kV/cm). The 1st (dashed line) and the 5th (dotted line) drift velocity harmonic amplitudes are shown for comparison.

Fig. 17. The 3rd harmonic drift velocity amplitude (solid line) as a function of the pumping wave frequency in n-type InP at $T = 300$ K. The curve labels give the wave electric field amplitude (in kV/cm). The 1st (dashed line) and the 5th (dotted line) drift velocity harmonic amplitudes are shown for comparison.

Fig. 18. Joule loss of the pumping wave power divided by the loss in n-type Si at room temperature as a function of the pumping wave amplitude. The curve labels give materials and lattice temperatures.

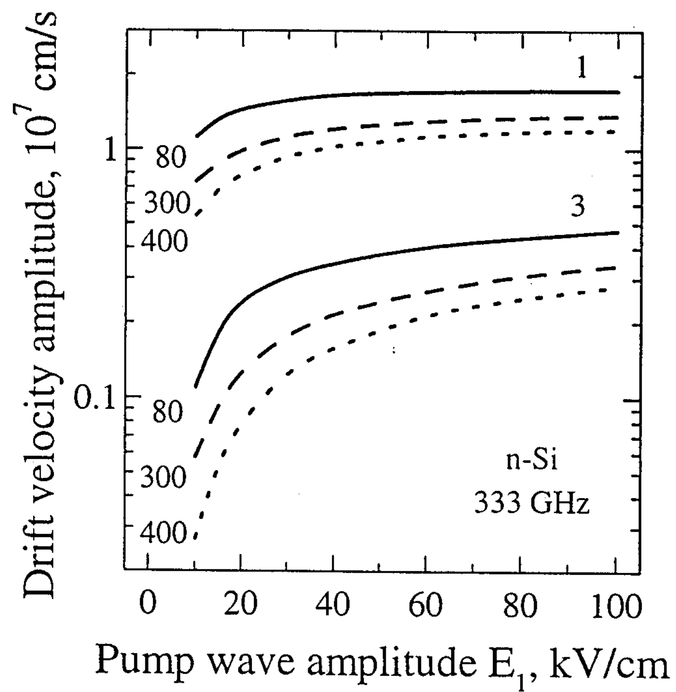

Fig. 1

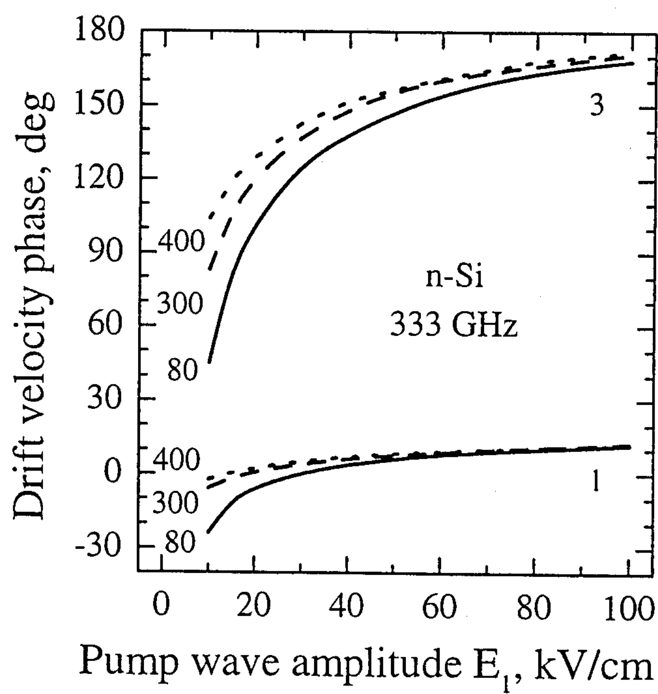

Fig. 2

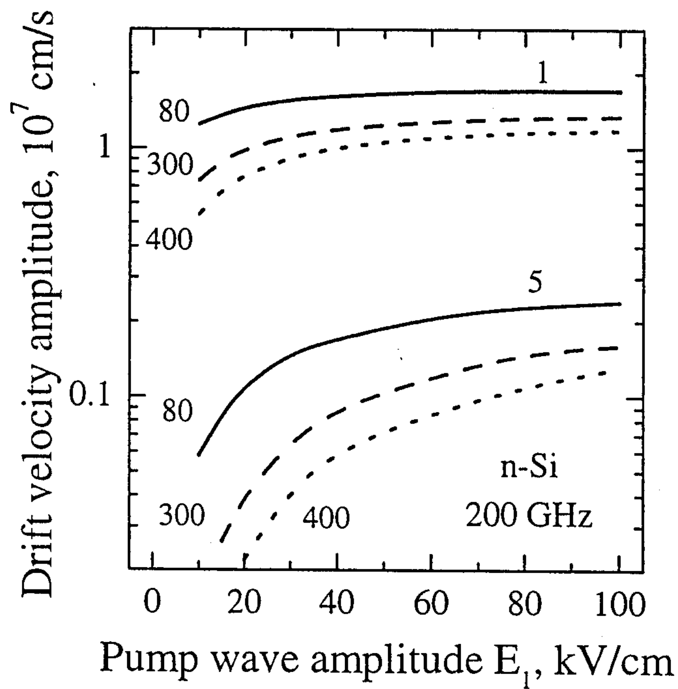

Fig. 3

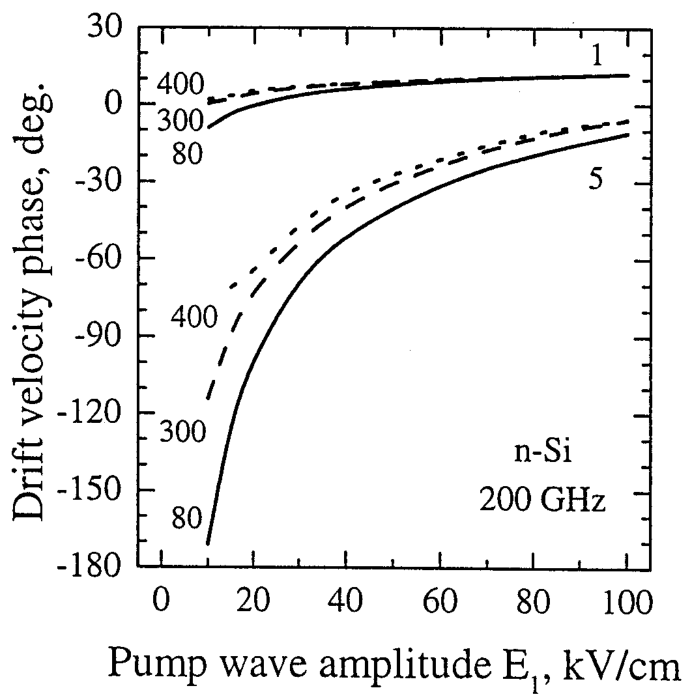

Fig. 4

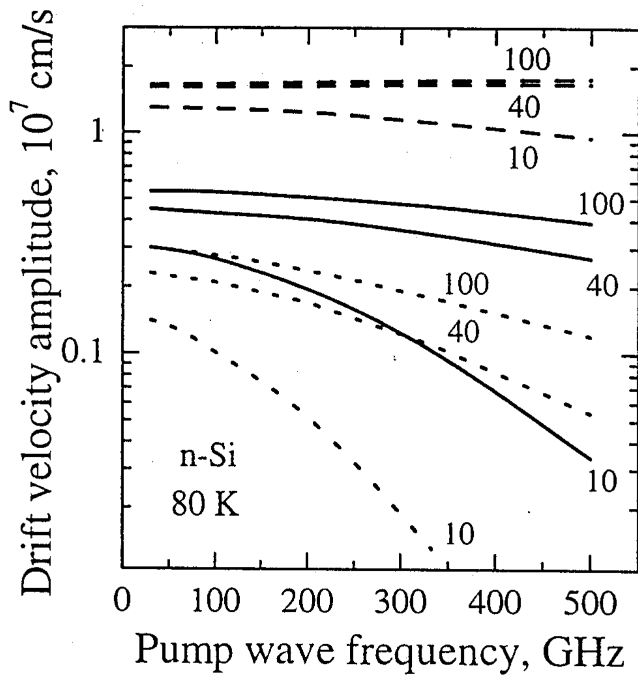

Fig. 5

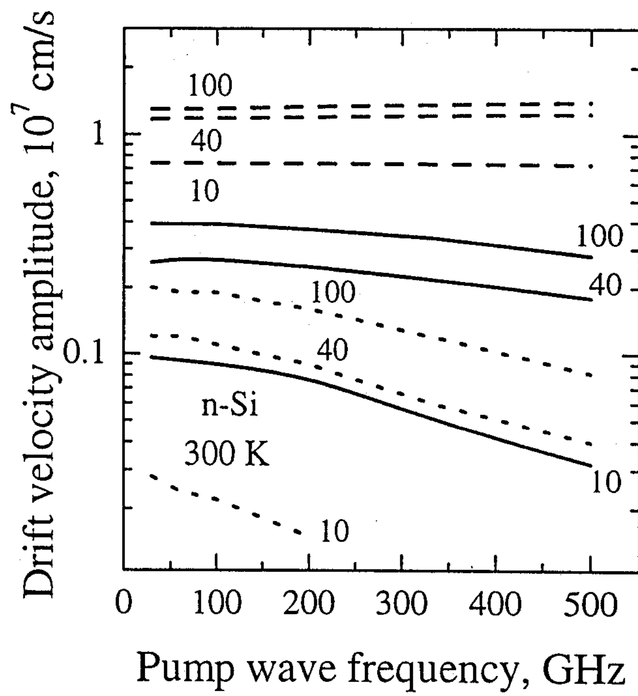

Fig. 6

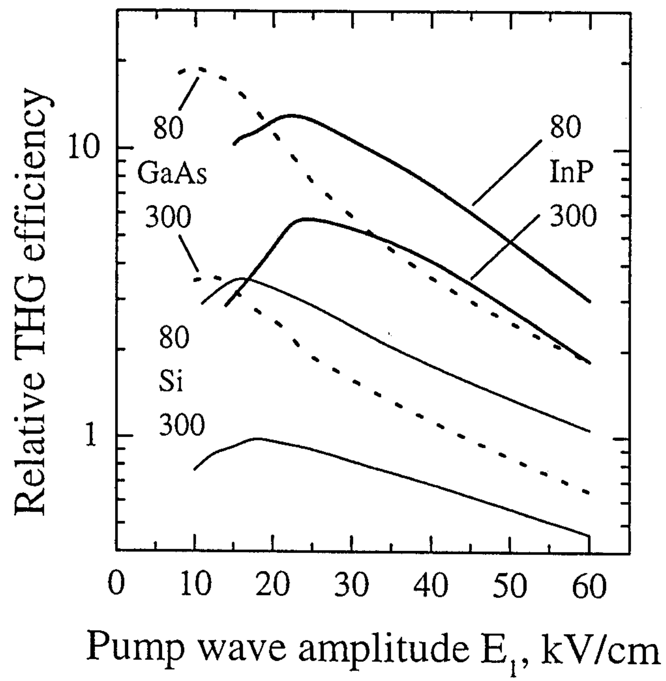

Fig. 7

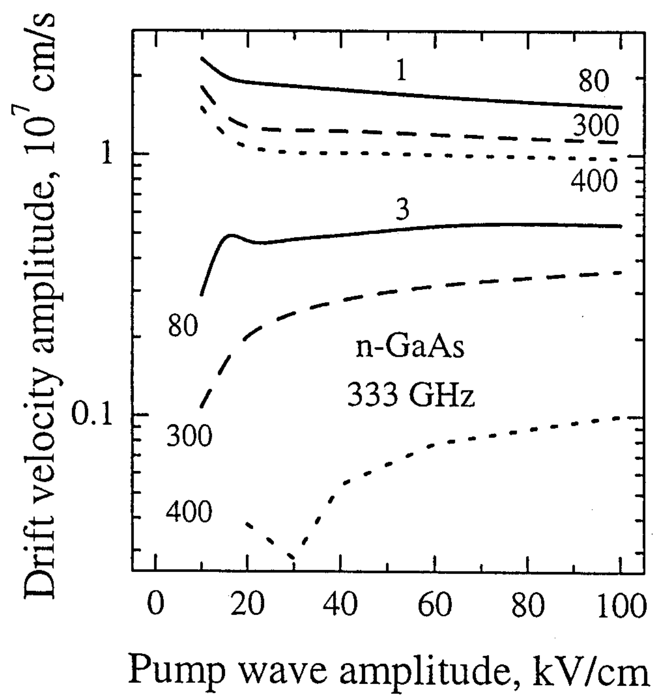

Fig. 8

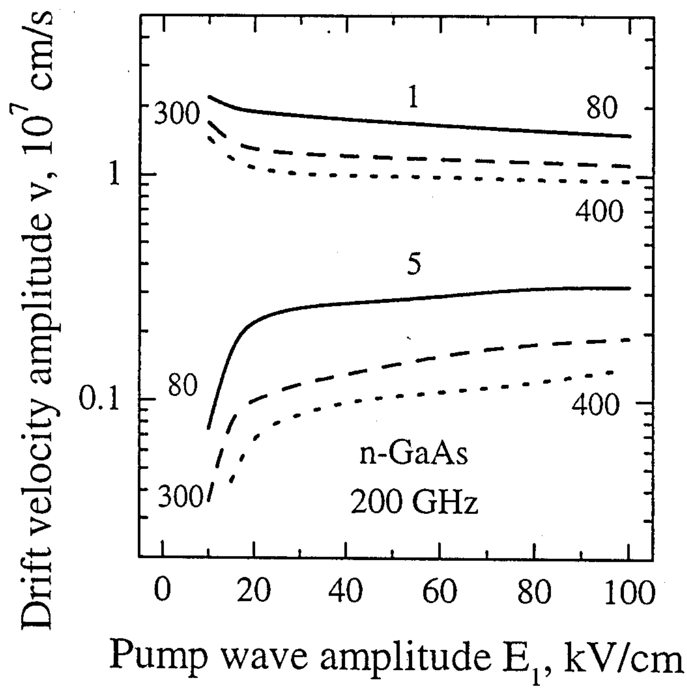

Fig. 9

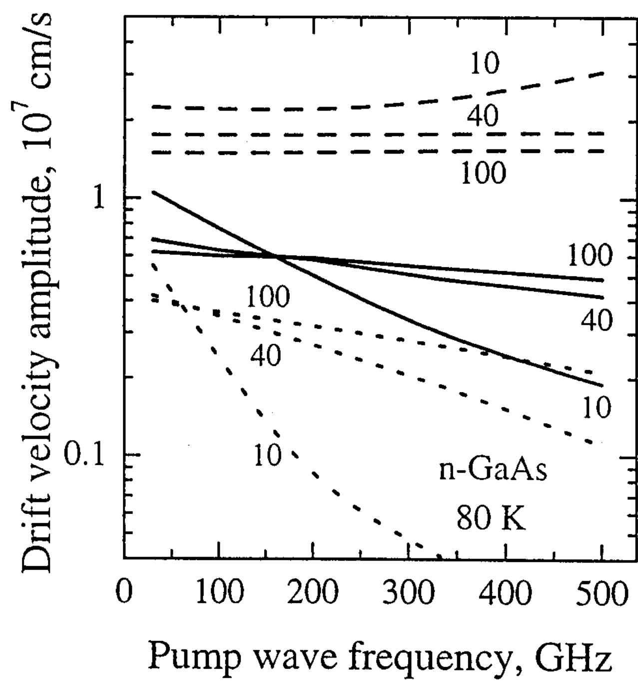

Fig. 10

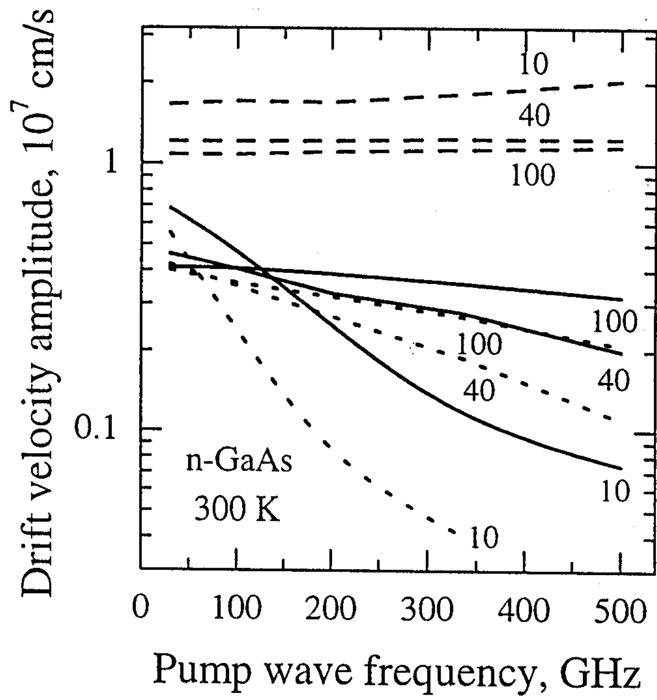

Fig. 11

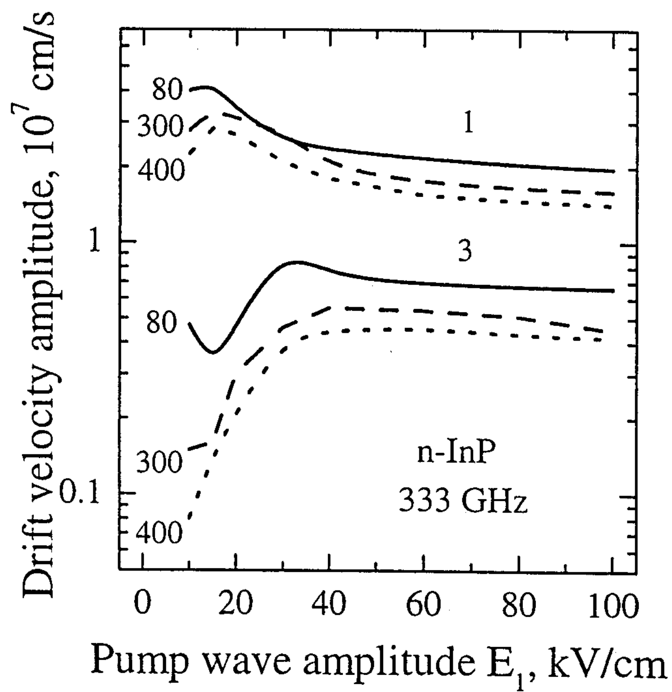

Fig. 12

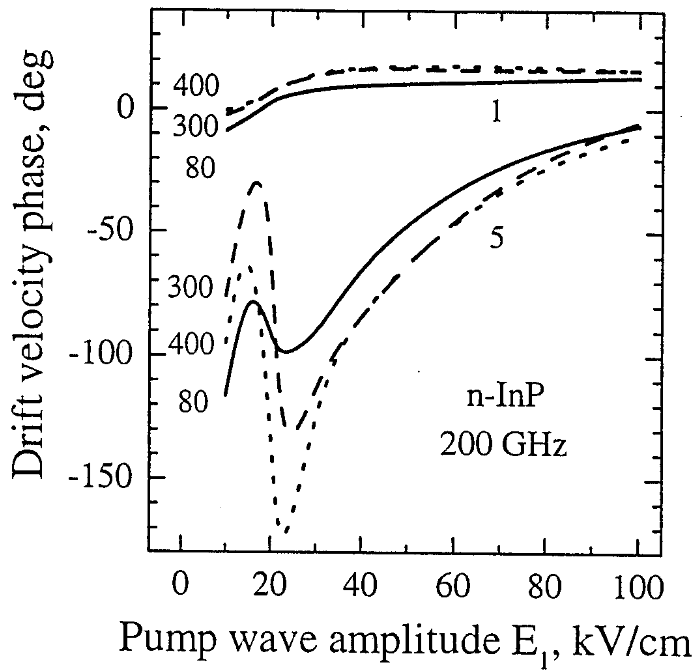

Fig. 15

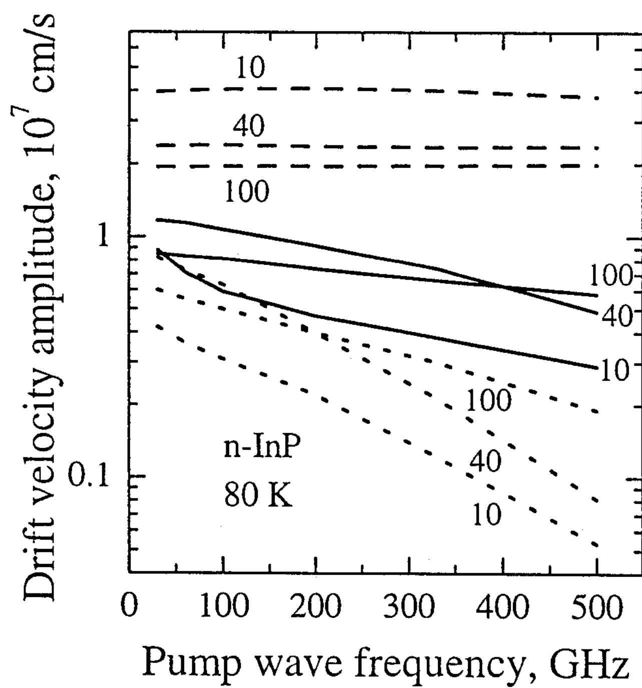

Fig. 16

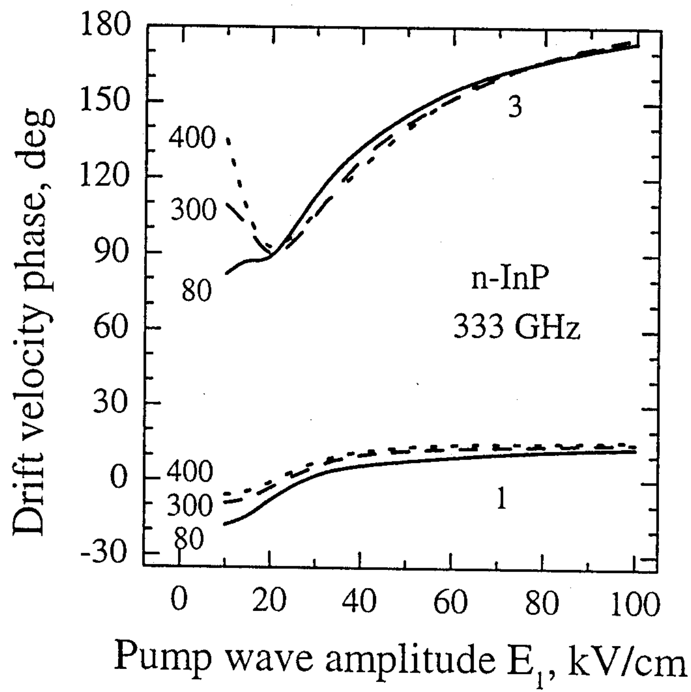

Fig. 13

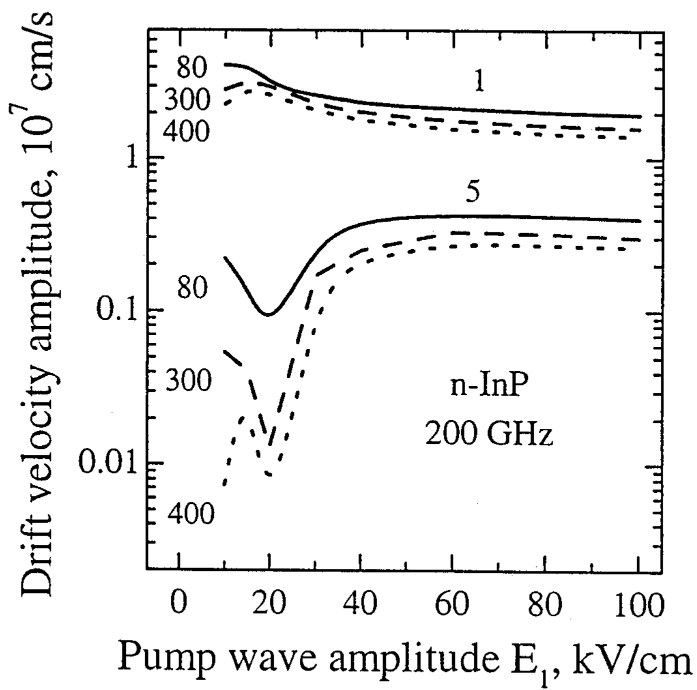

Fig. 14

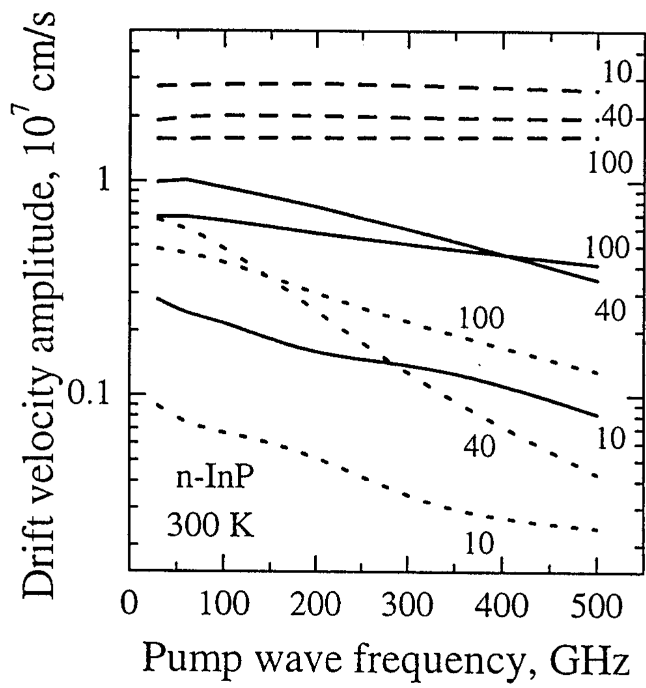

Fig. 17

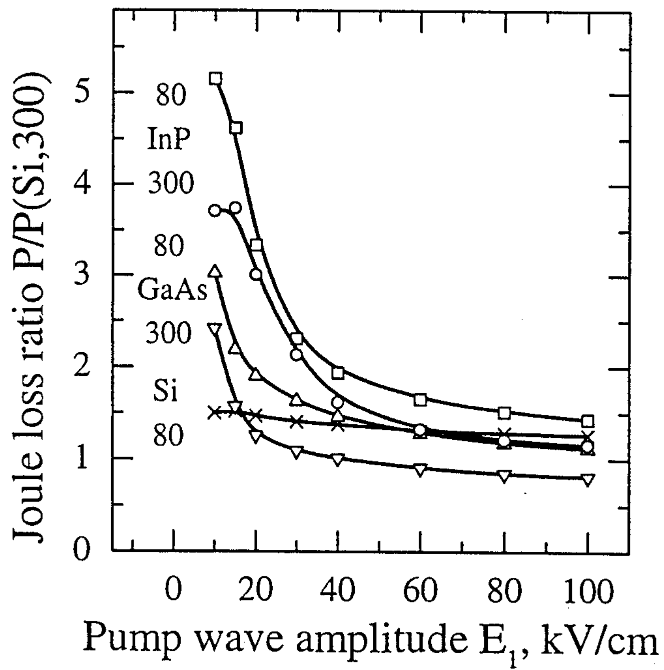

Fig. 18